Clinical breast imaging using sound-speed reconstructions of ultrasound tomography data

Cuiping Li[a], Neb Duric[b], and Lianjie Huang[c]
[a]Karmanos Cancer Institute, 4100 John R. Street, 4 HWCRC, Detroit, MI 48201; Phone: 313-576-8768, Emails: lic@karmanos.org
[b]Karmanos Cancer Institute, 4100 John R. Street, 4 HWCRC, Detroit, MI 48201; Phone: 313-576-8706, Emails: duric@karmanos.org
[c]Mail Stop D443, Los Alamos National Laboratory, Los Alamos, NM87545; Phone: 505-665-1108; Email: ljh@lanl.gov

ABSTRACT

To improve clinical breast imaging, a new ultrasound tomography imaging device (CURE) has been built at the Karmanos Cancer Institute. The ring array of the CURE device records ultrasound transmitted and reflected ultrasound signals simultaneously. We develop a bent-ray tomography algorithm for reconstructing the sound-speed distribution of the breast using time-of-flights of transmitted signals. We study the capability of the algorithm using a breast phantom dataset and over 190 patients' data. Examples are presented to demonstrate the sound-speed reconstructions for different breast types from fatty to dense on the BI-RADS categories 1-4. Our reconstructions show that the mean sound-speed value increases from fatty to dense breasts: $1440.8\,m/s$ (fatty), $1451.9\,m/s$ (scattered), $1473.2\,m/s$ (heterogeneous), and $1505.25\,m/s$ (dense). This is an important clinical implication of our reconstruction. The mean sound speed can be used for breast density analysis. In addition, the sound-speed reconstruction, in combination with attenuation and reflectivity images, has the potential to improve breast-cancer diagnostic imaging. The breast is not compressed and does not move during the ultrasound scan using the CURE device, stacking 2D slices of ultrasound sound-speed tomography images forms a 3D volumetric view of the whole breast. The 3D image can also be projected into a 2-D "ultrasound mammogram" to visually mimic X-ray mammogram without breast compression and ionizing radiation.

Keywords: Breast imaging, sound-speed reconstruction, ultrasound tomography.

1. INTRODUCTION

Breast cancer affects one in eight women during their lives. It is the most common cancer, and the second most common cause of cancer death in women. Recent studies have demonstrated the effectiveness of ultrasound imaging in detecting breast cancer [1-4]. The work of Greenleaf *et al.*[1] showed that ultrasound transmission parameters (sound-speed and attenuation) can help differentiate benign from malignant masses. To record both the transmitted and reflected ultrasound energy, a clinical ultrasound ring array scanner for breast cancer diagnosis, termed Computed Ultrasound Risk Evaluation (CURE), was designed and built at the Karmanos Cancer Institute (KCI) (Fig. 1)[4].

Since most abnormal breast masses have higher sound-speed than normal breast tissue, one of the primary purposes of the CURE device is to be able to accurately and efficiently produce images of breast sound-speeds based on the ultrasound signals that are transmitted through the breast tissue to the other side of the ring array. Therefore, a robust ultrasound sound-speed tomography algorithm is critical to ensure a high-resolution sound-speed reconstruction of the breast data. In combination with attenuation and reflection images, the sound-speed reconstructions can be used to differentiate benign masses from cancerous masses, and can improve the diagnostic ability and clinical utility of CURE. Furthermore, it has been shown that the sound speed correlates with the tissue density. Hence sound speed imaging can be used to accurately trace the glandular tissue of the breast and to potentially measure breast cancer risk [5].

Medical Imaging 2008: Ultrasonic Imaging and Signal Processing, edited by Stephen A. McAleavey, Jan D'hooge, Proc. of SPIE Vol. 6920, 692009, (2008) · 1605-7422/08/$18 · doi: 10.1117/12.771436

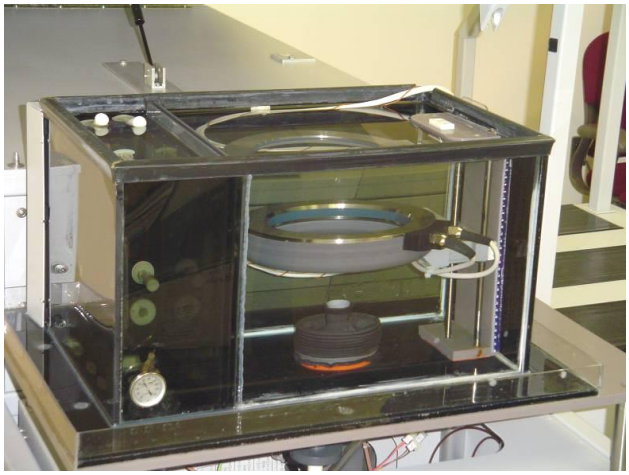

Figure 1. A picture of CURE transducer ring array.

In this paper, an iterative regularized refraction tomography method is implemented to extract sound-speed information from the ultrasound breast data acquired by CURE. In this tomography method, the ray bending effect is taken into consideration. Data from an anthropomorphic breast phantom and more than 190 patients acquired by CURE are reconstructed using this algorithm.

2. PATIENT SELECTION AND DATA COLLECTION

2.1 Patient selection

Our patient recruitment taps into the standard patient flow of KCI's Alexander J. Walt Breast Center. The CURE ultrasound exam is performed between mammography/standard ultrasound (US) exams and the US guided biopsy.

2.2 The CURE device and data collection

Figure 1 is a schematic representation of the CURE ring transducer. The 20-cm-diameter ring consists of 256 equally-spaced and water-coupled transducers, and is immersed into a water tank. During the scan, the patient is positioned prone with the breast situated through a hole in the canvas bedding. This results in the breast being suspended in water, inside the imaging tank, and also encircled by the ring. A motorized gantry translates the ring in the vertical direction, starting from the chest wall through the breast's nipple region. One complete scan takes about 1 minute, and leads to approximately 45-76 slices of data per patient.

During scanning at each slice, the 256 transducer elements sequentially emit fan beam ultrasound signals with a central frequency of 1.5 MHz toward the opposite side of the ring. The forward scattered (transmission) and backscattered (reflection) ultrasound signals are subsequently recorded by all 256 elements at a sampling rate of 6.25 MHz, and the data is used to reconstruct images of acoustic properties inside the breast.

3. ULTRASOUND SOUND-SPEED TOMOGRAPHY

Based on the Radon transform, classical tomography reconstruction using Filtered back-projection cannot take ray bending into account. However, ultrasound rays in inhomogeneous medium (such as breast tissue) are bent based on Fermat's Principle and Snell's Law. In this study, an iterative bent-ray ultrasound tomography algorithm with a new regularization term is used. To solve the problem of bent-ray ultrasound tomography, a regular rectangular grid model is created on the image plane, whose boundaries enclose the transducer ring. During each iteration, both the forward problem and the inverse problem are solved, and the sound-speed model is updated for the successive iterations. We describe the forward and inverse problems in the following.

3.1 Forward modeling

2-D ultrasound wave propagation is governed by the eikonal equation

$$(\nabla E)^2 = (\partial T / \partial x)^2 + (\partial T / \partial y)^2 = (1/v)^2 = (s_x^2 + s_y^2), \quad (1)$$

where T is the travel-time, v is the sound-speed, and (s_x, s_y) is the slowness vector of ultrasound wave that is defined as the reciprocal of the sound speed. In eq. (1), $E = const.$ describes the 'wavefronts', and 'rays' are defined as the orthogonal trajectories of these wavefronts.

Equation (1) can be solved using Klimes' grid travel-time tracing technique[6], which has been proven to be both accurate and fast. Klimes' method calculates the slowness vector (s_x, s_y) and travel-time T at the center point of each grid cell simultaneously with at least second-order accuracy (relative to the grid spacing). (s_x, s_y) and T at an arbitrary point within the grid model are interpolated by 2-D fourth order Lagrange interpolation. An ultrasound ray is backprojected from receiver to transmitter in the following way:

(1) Starting from the receiver location (x_r, y_r), the ray segment within the current grid cell is traced along the direction $\bar{G} = (-s_{x_r}, -s_{y_r})$ until it intercepts the cell boundary at point (x_i, y_i);

(2) Update $\bar{G}$ to be the negative slowness vector of the intercept point $\bar{G} = (-s_{x_i}, -s_{y_i})$, and trace the ray segment within the next adjacent cell;

(3) Repeat (2), until the current traced ray arrives at the transmitter.

3.2 Inverse problem

Let δt_i be the difference between the i^{th} picked time-of-flight for the recorded ultrasound data and the i^{th} calculated time-of-flight for the sound-speed model, our inverse problem can be described as follows

$$\sum_j^M l_{ij} \Delta s_j = \Delta t_i, \quad (2)$$

where Δs_j is the slowness perturbation for the j^{th} grid cell, which needs to be inverted, and l_{ij} is the ray length of the i^{th} ray within the j^{th} cell. Equation (2) can be expressed as a matrix form

$$L\delta S = \delta T. \quad (3)$$

This is a nonlinear inverse problem due to ray bending. A regularized tomography inversion algorithm is used to solve for δS

$$\delta S = (L^* C_d^{-1} L + \alpha C_{x_0}^{-1} + \beta I)^{-1} L^* \delta T, \quad (4)$$

where C_d^{-1} is the inverse data covariance matrix, $C_{x_0}^{-1}$ is the inverse a priori model covariance matrix, α and β are regularization parameters that balance the smoothness of the inverted results and the fit to the data. We choose a diagonal data weighting matrix C_d^{-1} whose diagonal elements are defined as

$$(C_d^{-1})_{ii} = 1/\varepsilon_i, \quad (5a)$$

where ε_i is the data error for the i^{th} ray. The regularization term $C_{x_0}^{-1}$ is defined as

$$C_{x_0}^{-1} = \sqrt{diag(L^* L)}, \quad (5b)$$

whose diagonal element $\sum_{i=1}^{m} l_{ij}^2$ is the total ray length within the j^{th} grid cell that renormalizes the inverse problem for unequal ray coverage. To compensate those grid cells without any ray coverage, an extra smoothing term (βI) is added to the inverse part in eq. (4).

To avoid computationally expensive matrix inversion, Paige and Saunders' LSQR method[7] is used to iteratively solve the nonlinear problem in eq. (4) for δS, starting with a homogeneous sound-speed model. After each iteration, an updated model is obtained by adding the solution δS to the initial model. Rays are traced on the updated model using the method discussed in the forward modeling section, and the time-of-flight data are updated at the same time. The iteration continues until the time-of-flight misfit δT does not decrease significantly from the previous iteration, which means the solutions have converged.

3.3 *In vitro* and *in vivo* datasets

The above tomogoraphy algorithm is applied to *in vitro* (breast phantom) data and *in viv*o breast datasets to image their sound-speed properties. The breast phantom was built by Dr. Ernest Madsen of the University of Wisconsin. It provides tissue-equivalent scanning characteristics of highly scattering, predominantly parenchymal breast tissue. A cross-section of X-ray CT scan is shown in Fig. 2a, which includes a subcutaneous fat layer, two fat inclusions (black), and two tumors (white).

All of the patients in this study were scanned with our clinical ultrasound prototype. All scanning procedures were performed under an institutional review board approved protocol and in compliance with the Health Insurance Portability and Accountability Act (HIPPA). The patient population provided a variety of breast types, breast mass types and sizes.

4. RESULTS

4.1 *In vitro* study

We apply our ultrasound tomography algorithm to a breast phantom dataset acquired using the CURE device. A phantom's cross-sectional CT scan and reconstructed sound-speed are shown in Figs. 2(a) and (b), respectively. Table 1 is a comparison between the reconstructed sound-speeds and their known sound-speeds. It shows that the sound-speed discrepancy is about 5 m/s. For small inclusions, the differences tend to be bigger (15 m/s for 6 mm mass and 19 m/s for 9 mm mass). The phantom results provide a general calibration for the imaging capability of our tomography algorithm using the CURE data.

4.2 *In vivo* study

More than 190 *in vivo* datasets acquired by CURE are reconstructed for the sound-speed distributions within the breast. The clinical protocol was designed to include a sample of patients with a wide variety of breast types, ranging from fatty to dense on the BI-RADS categories 1-4. Figure 3 presents examples of our sound-speed reconstructions for different breast types. Figure 3(a) shows a fatty breast as classified in the clinical mammogram report. Figure 3(b) illustrates the sound-speed distribution for a scattered breast with an irregular 1.2 cm invasive ductal carcinoma at 1:00 o'clock position as described in mammogram report. The breast in Fig. 3(c) is composed of heterogeneously dense fibroglandular tissue. The breast in Fig. 3(d) is a dense breast. Since the resolution limitation of our algorithm is about 3 wavelengths (4-5 mm), we do not expect our sound-speed reconstruction to be sensitive to the fibrous structure of the breast. However, as the images indicate, fatty and glandular tissues are well characterized.

Table 1. Comparison of reconstructed sound-speeds with known sound-speeds for a breast phantom.

Material	Diameter (*mm*)	Known (m/s)	Calculated (m/s)	Difference (m/s)
Big fat sphere	12	1470	1468	2+
Small fat sphere	6	1470	1485	15-
Subcutaneous fat	9	1470	1468	2+
Glandular	15	1515	1512	3+
Small tumor		1549	1530	19+
Irregular tumor		1559	1555	4+

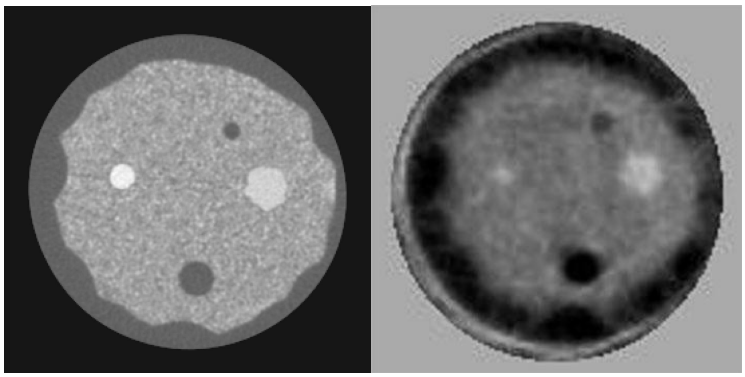

(a) (b)

Figure 2. (a) A cross-section of X-ray CT scan of the breast phantom. (b) Sound-speed reconstruction of the same cross-section.

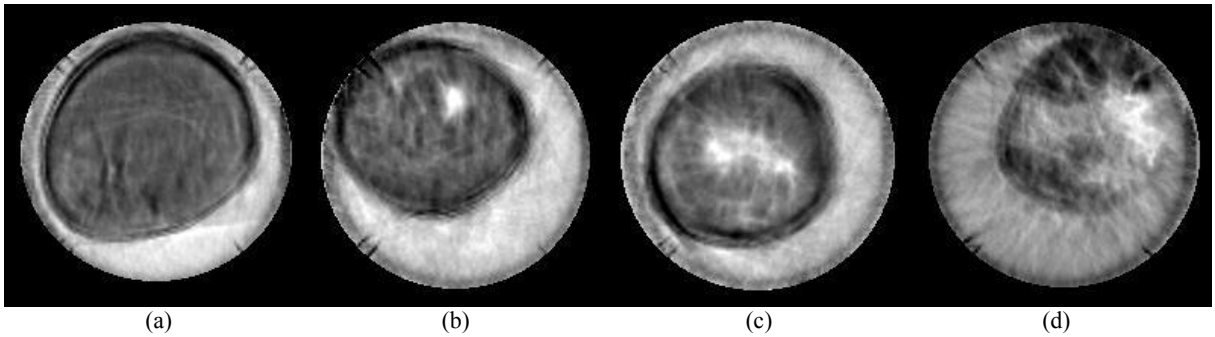

(a) (b) (c) (d)

Figure 3. (a) Sound-speed reconstruction for a fatty breast. (b) Sound-speed reconstruction for a breast with scattered fibroglandular tissue. (c) Sound-speed reconstruction for a breast composed of heterogeneous dense fibroglandular tissue. (b) Sound-speed reconstruction for a dense breast.

We conduct further analysis to quantitatively correlate the breast type with sound-speed values. Sound-speed reconstructions for 74 breasts are analyzed to obtain the mean sound-speed values using the following procedure:
(1) For a single breast, the mean sound-speed of every 5 slices is calculated by averaging the whole area of the breast with the breast mass segmented out;
(2) The mean sound-speed of the whole breast is calculated by averaging the mean sound-speeds obtained in (1).

The analysis uses reconstructed sound-speeds for 27 fatty breasts, 14 breasts with scattered fibroglandular tissue, 18 heterogeneous dense breasts, and 15 breasts with dense fibroglandular tissue. The statistics of mean sound-speeds for different breast type is depicted in Fig. 4. Fatty breasts have a mean sound-speed of $1440.8\,m/s$, while mean sound-speeds for scattered, heterogeneous, and dense breasts are $1451.9\,m/s$, $1473.20\,m/s$, and $1505.25\,m/s$, respectively. The solid breast masses usually have higher sound-speed than the surrounding tissue, which, in most cases,

can be detected by sound-speed reconstruction. However, we do not rely on sound-speed reconstruction to differentiate the types of breast masses due to their subtle sound-speed differences.

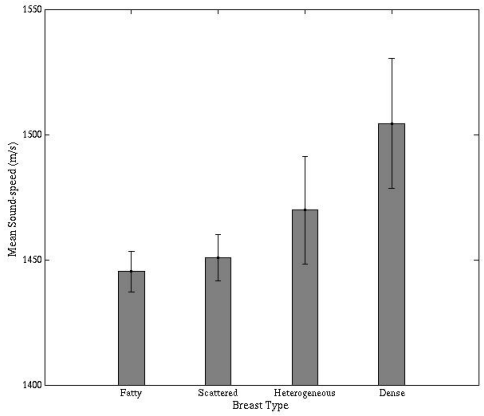

Figure 4. Box plot of mean sound-speed values for 74 patients categorized by BI-RADS as fatty, scattered, heterogeneous, and dense breast.

5. DISCUSSION AND CONCLUSIONS

During our patient recruiting, the CURE device was upgraded twice. Among our 190+ patients' data, 127 of them were scanned by two older transducer ring arrays which have an elevation beam width of 12 mm. Patients after that were scanned by a new transducer ring with an elevation beam width of 5 mm. The performance of our reconstruction algorithm declines when the mass size drops to and below the elevation beam width (12 mm for the old rings and 5 mm for the new ring), since the signal dilution leads to a loss of contrast. Another important factor influencing the performance of our algorithm is the signal-to-noise ratio of the acquired patient data. Low signal-to-noise ratio of the data affects the accuracy of our time-of-flight picks, and consequently degrades the sound-speed reconstructions.

As discussed previously, the CURE device scans the breast slice by slice. Therefore, like MRI, our sound-speed tomography can image the whole volume of the breast. Figure 5(a) is an example of mosaic composed of the sound-speed reconstructions for the entire 76 slices of a single breast scan starting from chest wall to nipple region. Stacking all 76 slices together gives a 3D volumetric image of the sound-speed reconstructions for the same breast (Fig. 5b).

The volumetric information can benefit further upstream research. We have shown above that for our current patient population, the sound-speed reconstructions can detect the majority of the breast masses due to their higher sound-speed values. Moreover, in combination with CURE attenuation and reflection images, sound-speed measurements can be used to differentiate breast mass types. Statistically, the malignant masses have elevated sound-speed and attenuation relative to surrounding tissue. The architectural distortion at the tumor region in the reflection image is another indicator of cancer[8]. Fusing sound-speed, attenuation and reflection images together can visually enhance the breast mass. The fused image for the patient in Fig. 5 is illustrated in Fig. 6 which shows a local enhancement at the tumor location. The inverted RGB instead of RGB is used to obtain a visually better fused image.

To mimic X-ray mammogram, the 3D volumetric sound-speed image can be projected into two dimensional images of different views to form "ultrasound mammogram." The Z-project function of ImageJ (a freeware available at http://rsb.info.nih.gov/ij) is used for the projection. Some examples of variable breast type ranging from fatty to dense on the BI-RADS categories 1-4 are shown in Fig. 7 (from left to right breast types are fatty, scattered, heterogeneous, and dense, respectively). Figures 7(a) and (b) illustrate the CC views of "ultrasound mammogram" using the maximum intensity projection and average intensity projection, respectively.

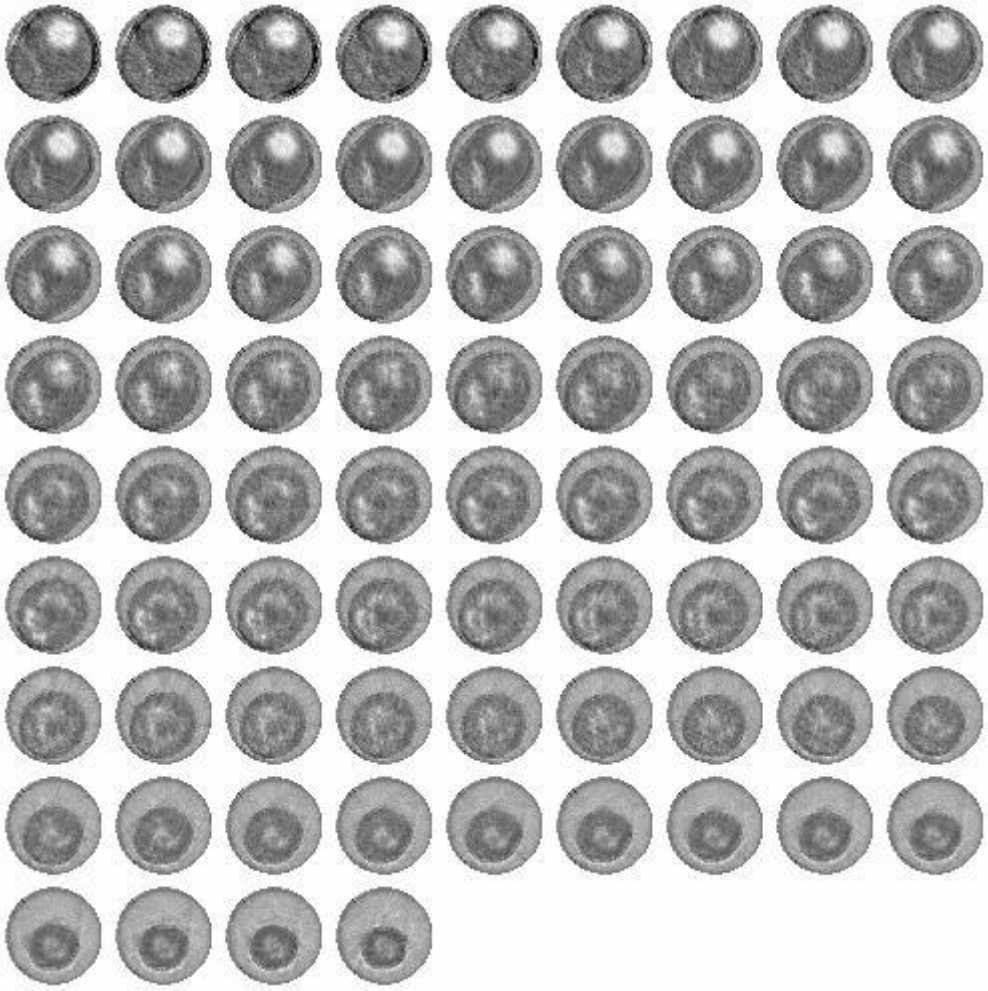

(a)

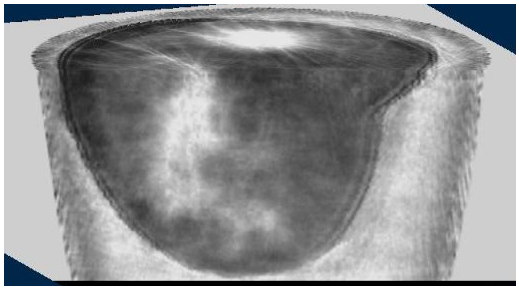

(b)

Figure 5. Volume rendering of CURE sound-speed images. (a) Mosaic composed of sound-speed reconstructions for all 76 slices of a single breast scan. (b) 3D volumetric view of the sound-speed reconstructions for the same breast as (a).

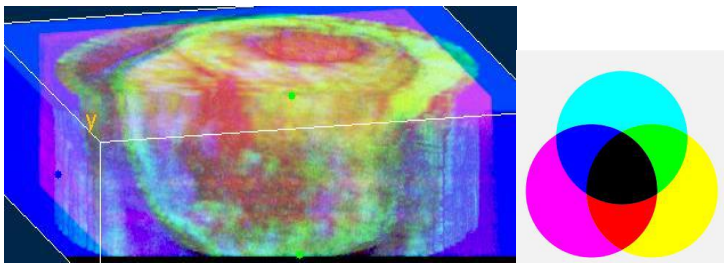

Figure 6. An example of fused CURE image. Left: fused image by superimposing sound-speed, attenuation and reflection images together; right: legend for the fused image where the sound-speed image is presented as pink (inverted green), attenuation as yellow (inverted blue), and reflection as greenish blue (inverted red).

Sound-speed imaging of breast data has additional potential clinical value. Glide *et al*.[5] studied the correlation between the sound-speed and the density of the breast and found that, in general, dense breast coincides with a high sound-speed. This correlation motivated their research on utilizing the whole-breast sound-speed as an overall indicator of the breast density that is a very important risk factor for breast cancer.

ACKNOWLEDGEMENTS

This work was supported through the Karmanos Cancer Institute and a grant from the Michigan Economic Development Corporation (Grant Number 06-1-P1-0653). L. Huang acknowledges the support of the U.S. DOE Laboratory-Directed Research and Development program at Los Alamos National Laboratory.

REFRENCES

1. Greenleaf, J. F., Johnson, A., Bahn, R. C. and Rajagopalan, B., "Quantitative cross-sectional imaging of ultrasound parameters," Ultrasounics Symposium Proceedings, 989-995 (1977).
2. Carson, P. L., Meyer, C. R., Schezinger, A. L. and Oughton, T. V., "Breast imagin in coronal planes with simultaneous pulse echo and transmission ultrasound," Science 214, 1141-1143 (1981).
3. Andre, M. P., Janee, H. S., Martin, P. J., Otto, G. P., Spivey, B. A. and Palmer, D. A., "High-speed data acquisition in a diffraction tomography system employing large-scale toroidal arrays," International Journal of Imaging Systems and Technology 8, 137-147 (1997).
4. Duric, N., Littrup, P., Poulo, L., Babkin, A., Pevzner, R., Holsapple, E., Rama, O. and Glide C., "Detection of breast cancer with ultrasound tomography: First results with the Computed Ultrasound Risk Evaluation (CURE) prototype," Medical Physics 3**4**, 773-785 (2007).
5. Glide, C., Duric, N. and Littrup, P., "Novel approach to evaluating breast density utilizing ultrasound tomography," Medical Physics 34, 744-753 (2007).
6. Klimes, L., "Grid Travel-time Tracing: Second-order Method for the first Arrivals in Smooth Media," Pageoph 148, 539-563 (1996).
7. Paige, C. C. and Saunder, M. A., "LSQR: An Algorithm for Sparse Linear Equations and Sparse Least Squares," ACM Transactions on Mathematical Software 8, 43-71 (1982).
8. Stavros, A. T., Thickman, D., Rapp, C. L., Dennis, M. A., Parker, M. A. and Sisney, G. A., "Solid breast nodules: use of sonography to distinguish between benign and maligmant lesions," Radiology 196, 123-134 (1995).

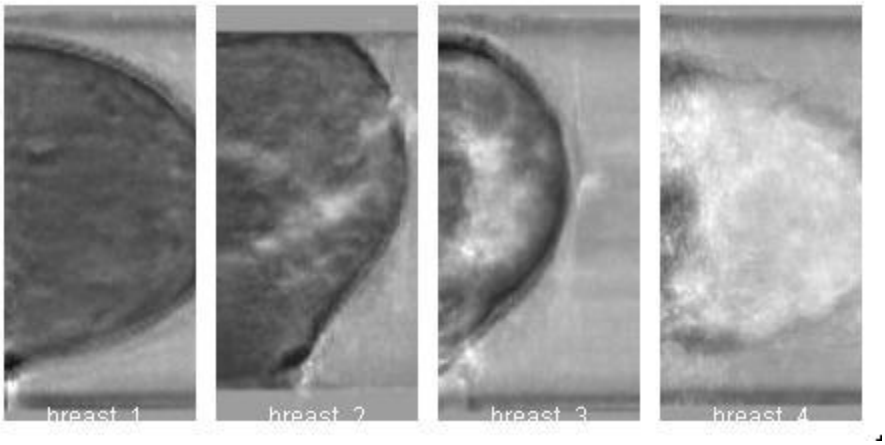

(a)

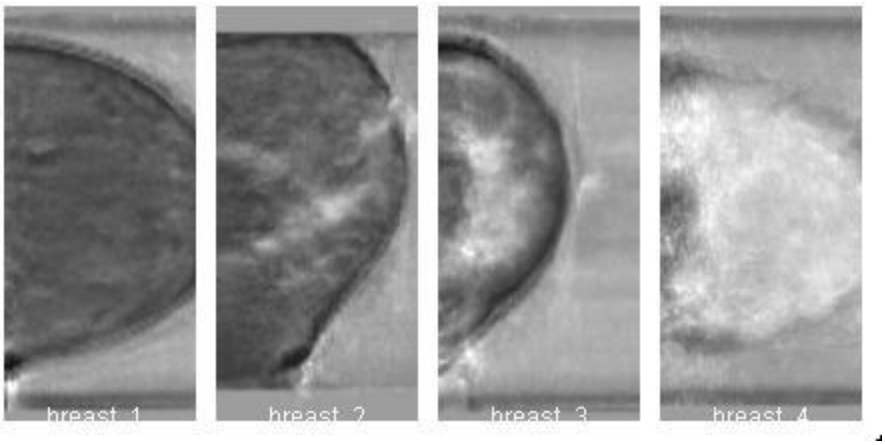

(b)

Figure 7. "Ultrasound mammograms" of breasts of different types ranging from fatty to dense on the BI-RADS categories 1-4 (from left to right, breast types are fatty, scattered, heterogeneous, and dense, respectively). (a) CC views using the maximum intensity projection. (b) CC views using the average intensity projection.